Available online at www.sciencedirect.com
ScienceDirect
International Journal of Heat and Mass Transfer 51 (2008) 3946–3952
International Journal of HEAT and MASS TRANSFER
www.elsevier.com/locate/ijhmt

Dimensionless correlations of frost properties on a cold cylinder surface

Jung-Soo Kim, Dong-Keun Yang, Kwan-Soo Lee *

School of Mechanical Engineering, Hanyang University, Sungdong-gu, Seoul 133-791, Republic of Korea

Received 24 May 2007; received in revised form 11 January 2008
Available online 4 March 2008

Abstract

We propose dimensionless correlations for frost properties on a cold cylinder surface. Frosting experiments were performed while changing various frosting parameters such as the air temperature, cold cylinder surface temperature, air velocity, and absolute humidity. The experimental data showed that a uniform frost layer grew around the circumference of the cylinder at a high air velocity. Dimensionless correlations for the thickness, density, and surface temperature of the frost layer, and for the heat transfer coefficient were obtained as functions of the Reynolds number, Fourier number, absolute humidity, and dimensionless temperature. The applicable ranges of these correlations are Reynolds number of 700–3000 (air velocities of 0.5–2.0 m/s), Fourier number of 56.8–295.7 (operating time of 0–100 min), absolute humidity of 0.00280–0.00568 kg/kg_a, air temperatures of 3–9 °C, and cold cylinder surface temperatures of −32 to −20 °C. The proposed correlations agreed with the experimental data within an error of 15%.

Keywords: Dimensionless correlation; Frost property; Cold cylinder surface

1. Introduction

The porous frost layer that forms on a heat exchanger operated under frosting conditions causes a decrease in the heat transfer rate because it acts as thermal resistance between the airflow and the cold surface of the heat exchanger. The thermal performance of the heat exchanger also degrades owing to the reduced airflow rate during frost formation. Previous studies have shown that the frost behavior depends on the operating conditions of the heat exchanger, demonstrating the importance of frost properties in designing heat exchangers.

Frost properties on a cold plate have been experimentally investigated in several studies [1–8]. Östin and Andersson [1] and Yonko and Sepsy [2] expressed the effective thermal conductivity of the frost layer as a function of the frost density. Tokura et al. [3] and Biguria and Wenzel [4] obtained correlations for the thickness, density, and effective thermal conductivity of the frost layer. Hosoda and Uzuhashi [5] derived correlations for the density and effective thermal conductivity of the frost layer by considering the cold surface temperature and the air velocity. Mao et al. [6,7] proposed dimensionless correlations for frost properties at very low-humidity, and Yang and Lee [8] derived dimensionless correlations for frost properties as functions of the frosting parameters. These previous studies have presented frost property correlations for a cold plate, but relatively little research have been conducted on a cold cylinder. Recently, evaporators have been designed using the increased heat transfer area of tubes compared to that of fins to improve their thermal performance and reduce their production cost. Consequently, it is necessary to evaluate frost formation phenomena on a cold cylindrical surface.

Most studies related to cylinders have focused on an analysis of the frost growth. Aoki et al. [9] presented a set of experimental data for the frost thickness, frost density, and heat transfer at different angular positions on a vertical cylinder, while Chung et al. [10] examined the effects of the air velocity and air humidity ratio on the heat and mass transfer. Lee and Ro [11] conducted an experimental study to predict the thickness and effective thermal

* Corresponding author. Tel.: +82 2 2220 0426; fax: +82 2 2295 9021.
E-mail address: ksleehy@hanyang.ac.kr (K.-S. Lee).

0017-9310/$ - see front matter © 2008 Elsevier Ltd. All rights reserved.
doi:10.1016/j.ijheatmasstransfer.2008.01.007

Nomenclature

A	area, m^2
c_p	specific heat, J/kg K
d	diameter of cylinder, m
Fo	Fourier number, $\alpha_a t/d^2$
h_h	heat transfer coefficient, W/m^2 K
h_m	mass transfer coefficient, kg/m^2 s
h_{sv}	latent heat of sublimation, J/kg
k	thermal conductivity, W/m K
m_f	frost mass, kg
$\dot{m}$	mass flow rate, kg/s
Nu	Nusselt number, $h_h d/k_a$
Q	heat transfer rate, W
r	radius of cylinder, m
Re_d	Reynolds number, $u_a d/v_a$
T	temperature, K
t	time, s
u_a	air velocity, m/s
W	length of cylinder, m
w_a	absolute humidity, kg/kg_a
y_f	frost thickness, m

Greek symbols

α	thermal diffusivity, m^2/s
v	dynamic viscosity, m^2/s
ρ	density, kg/m^3

Superscript

*	dimensionless

Subscripts

a	air
ave	average
c	cold surface
f	frost
fs	frost surface
ice	ice
in	inlet
out	outlet
r	refrigerant
tot	total
tp	triple point of water

conductivity of the frost layer on a horizontal cylinder, but these results were only applicable under low-humidity air conditions. Padki et al. [12] proposed a simple numerical model for the frost formation on a plate and a cylinder, and then predicted the thickness and surface temperature of the frost layer. Other studies [13–15] presented empirical correlations for the frost thickness on a cylinder. Cremers and Mehra [13] proposed a correlation for the frost thickness of free convective flow, which has only limited applications for forced convection. Schneider [14] proposed a correlation for the frost thickness without considering the air velocity, while Sengupta et al. [15] derived empirical heat transfer and frost thickness correlations that are only applicable to high-temperature air. Since the applicable operating conditions of the Sengupta et al. correlations are beyond the limits of conventional refrigerators and freezers, the use of these correlations for such devices may cause large errors. Thus, previous studies [9–15] related to frost formation with cylinders have only presented experimental data for limited frosting conditions, or frost thickness correlations only as functions of specific frosting parameters.

In this study, we performed frosting experiments on a cold cylinder surface under various frosting conditions. The local frosting behavior was determined for different angular positions. Correlations for the thickness, density, and surface temperature of the frost layer, and for the heat transfer coefficient were derived as functions of the Reynolds number, Fourier number, air humidity ratio, dimensionless air temperature, and non-dimensional cold cylinder surface temperature.

2. Experiments

The experimental apparatus used in this study consisted of a climate chamber to regulate the air temperature and humidity, a refrigeration section to maintain the flow rate and temperature of the refrigerant, a test section to perform the frosting experiments, and a circulation section to adjust the airflow rate and to connect each section, as shown in Fig. 1. Each section of the apparatus was independently controllable [8]. Fig. 2a shows a schematic diagram of the test section used to predict frosting behavior on a cold cylinder. The test section ($L \times W \times H = 400 \times 150 \times 150$ mm) was made of transparent acryl, and a stainless steel cylinder with an outer diameter (d) of 20 mm was placed in the center of the test section. As shown in Fig. 2b and c, the cylinder is rotated for frost thickness measurement only.

RTD sensors of Pt 100 Ω in a dry/wet bulb thermometer were installed inside the climate chamber to measure the temperature and humidity of the moist air. The air was regulated by a PID controller, heater, cooler, and humidifier. The refrigeration section consisted of a refrigerator and a pump to circulate the refrigerant. A solution of ethylene glycol and distilled water at a mass ratio of 6:4 was used as the refrigerant. The air temperatures at the inlet and outlet of the test section and the cold cylinder surface temperature were measured with type-T thermocouples or thermopiles, and humidity sensors were used to measure the air humidity. The airflow rate was controlled by a blower with an inverter and measured using a flow nozzle. To homogenize the airflow, a honeycomb and an air mix-

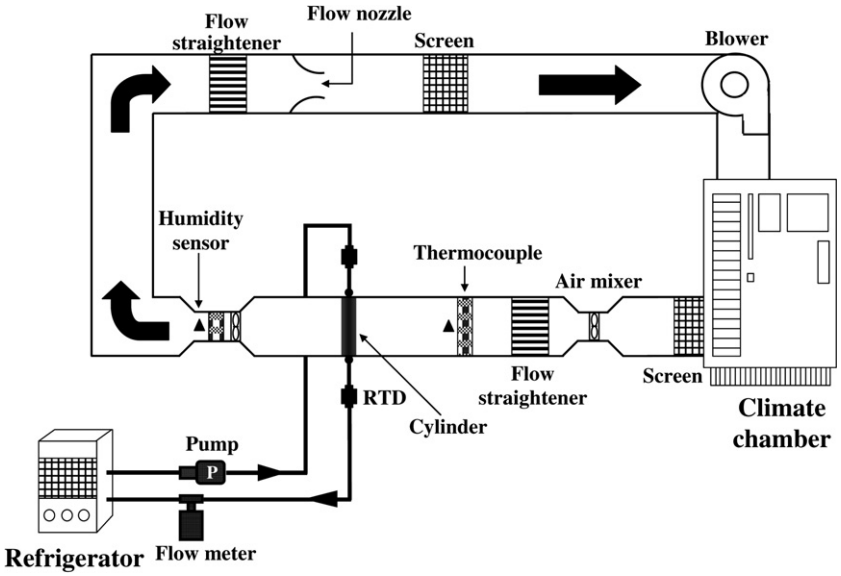

Fig. 1. Schematic diagram of the experimental apparatus.

ing fan were installed at the inlet and outlet of the test section, respectively. Insulating material was placed on the surface of the experimental apparatus to minimize heat loss.

Aluminum tape for weighing the frost mass was placed on the surface of the horizontal cylinder before the start of the experiment. The cold surface was also covered with plastic wrap to prevent frost formation until steady-state experimental conditions were reached, which were then controlled by the refrigerator, pump, and climate chamber. The plastic wrap on the cold surface was removed after conditions reached a steady-state, at which point the frosting experiments were started. Primary experimental data, such as the air temperature and humidity, cold cylinder surface temperature, airflow rate, and refrigerant temperature, were recorded every 4s by a data recording system connected to a personal computer. This study performed frosting experiments independently for operation times of 20, 40, 60, 80, and 100 min, measuring the frost properties. The frost thickness and frost mass were measured as soon as the frost surface temperature was recorded at the end of each operation time. Each experiment was repeated more than five times to check repeatability.

A digital micrometer was used to measure the frost thickness every 30° around the circumference of the cylinder by rotating the cylinder, as shown in Fig. 2b. The micrometer probe was made of acrylic resin to prevent the melting of the frost when it touched the frost surface. To identify whether the tip of the probe touched the frost surface or not, the tip was colored black and observed with a magnifier. The frost surface temperature was measured at 45° intervals using an infrared thermometer with the cylinder fixed in position without rotation, as shown in Fig. 2a and c. To minimize the sensitivity of the thermometer to the measurement angle, we maintained the measurement angle at 90° to the cylinder surface (for 45°, 90°, and 135°) by placing holes through which infrared emitted from the thermometer could contact the cylinder. We measured the frost surface temperature through the side holes only for 0° and 180° to avoid perturbing the flow, keeping the thermometer as close as possible to perpendicular to the cylinder. For the frost mass measurements, we removed the aluminum tape from the cylinder at 90° intervals as shown in Fig. 2c, and measured the frost weight formed on the aluminum tape using a chemical balance. The reason for the 90° interval was to reduce the error in frost mass measurement caused by a small angle.

The frost density was calculated from the frost thickness and frost mass,

$$\rho_f = \frac{m_f}{\pi[(r+y_f)^2 - r^2]W} \tag{1}$$

where r and W are the radius and length of the cylinder, respectively.

The air-side heat transfer rate was computed using the airflow rate and the temperature and humidity differences between the inlet and outlet of the test section,

$$\begin{aligned} Q_{tot} &= Q_{sen} + Q_{lat} \\ &= \dot{m}_a c_{p,a}(T_{a,\,in} - T_{a,\,out}) + \dot{m}_a(w_{a,\,in} - w_{a,\,out})h_{sv} \\ &= h_h A_{tot}(T_{a,\,ave} - T_{fs}) + h_m A_{tot}(w_{a,\,ave} - w_{fs})h_{sv} \end{aligned} \tag{2}$$

where Q_{sen} and Q_{lat} are the sensible heat and latent heat transfer, respectively.

The heat transfer rate for the refrigerant was obtained from

$$Q_{tot} = \dot{m}_r c_{p,r}(T_{r,out} - T_{r,in}) \tag{3}$$

As required by ASHRAE Standard 33–78, the energy balance between the air and the refrigerant was maintained within a maximum error of 5% during the experiments. The average heat and mass transfer coefficients for the cold

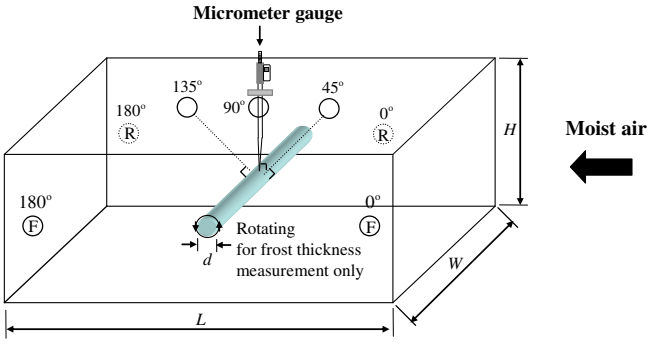

(a) Schematic diagram of the test section.

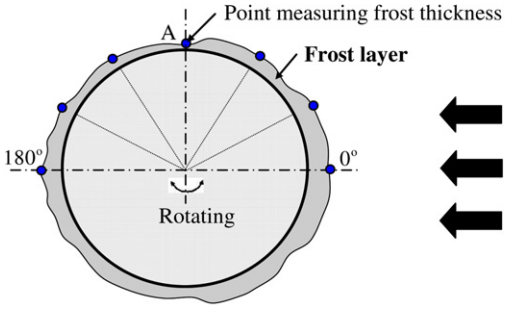

(b) Frost thickness

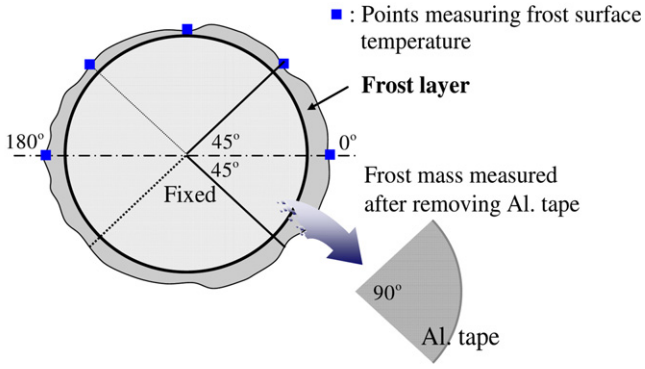

(c) Frost surface temperature and frost mass

Fig. 2. The test section and cross-sectional area of a cylinder showing measurement points.

cylinder were calculated from the experimental data as follows:

$$h_h = \frac{\dot{m}_a c_{p,a}(T_{a,\,in} - T_{a,\,out})}{A_{tot}(T_{a,\,ave} - T_{fs})} \quad (4a)$$

$$h_m = \frac{\dot{m}_a(w_{a,\,in} - w_{a,\,out})}{A_{tot}(w_{a,\,ave} - w_{fs})} \quad (4b)$$

The uncertainties in the experimental data were determined by considering the bias error and the accuracy of the measuring devices [16]. The uncertainties of the average frost thickness, frost density, frost surface temperature, and heat transfer coefficient were 5.3%, 6.6%, 4.6%, and 5.1%, respectively.

3. Results and discussion

The Frosting experiments were conducted to obtain frost property correlations on a horizontal cold cylinder. Table 1 shows the experimental conditions for 33 cases, which were selected based on the design of experiment.

3.1. Local frosting behavior with angular position

We measured the local thickness, density, and surface temperature of the frost layer that formed on the horizontal cylinder surface.

Figs. 3 and 4 show the temporal variations in the local frost thickness with angular position for low and high air velocities, respectively. The characteristics of the local frost growth at a low air velocity were similar to the heat transfer characteristics under non-frosting conditions [17]. For a low air velocity, the heat and mass transfer at the front of the cylinder were very active due to the collision of high-temperature moist air, and were inactive beyond the separation point. The generation and growth of a vortex flow caused an increase in the frost thickness at the rear stagnation point. However, the frost layer thickness grew uniformly around the cylinder at a high air velocity.

Table 1
Test conditions

Run	T_a (°C)	u_a (m/s)	w_a (kg/kg$_a$)	T_c (°C)
1	3	0.50	0.00280	−32
2	3	0.50	0.00374	−32
3	9	0.50	0.00425	−32
4	9	0.50	0.00568	−32
5	3	2.00	0.00280	−32
6	3	2.00	0.00374	−32
7	9	2.00	0.00425	−32
8	9	2.00	0.00568	−32
9	3	0.50	0.00280	−20
10	3	0.50	0.00374	−20
11	9	0.50	0.00425	−20
12	9	0.50	0.00568	−20
13	3	2.00	0.00280	−20
14	3	2.00	0.00374	−20
15	9	2.00	0.00425	−20
16	9	2.00	0.00568	−20
17	6	1.25	0.00404	−26
18	3	0.50	0.00280	−26
19	3	0.50	0.00374	−26
20	9	0.50	0.00425	−26
21	9	0.50	0.00568	−26
22	3	2.00	0.00280	−26
23	3	2.00	0.00374	−26
24	9	2.00	0.00425	−26
25	9	2.00	0.00568	−26
26	3	1.25	0.00280	−32
27	3	1.25	0.00374	−32
28	9	1.25	0.00425	−32
29	9	1.25	0.00568	−32
30	3	1.25	0.00280	−20
31	3	1.25	0.00374	−20
32	9	1.25	0.00425	−20
33	9	1.25	0.00568	−20

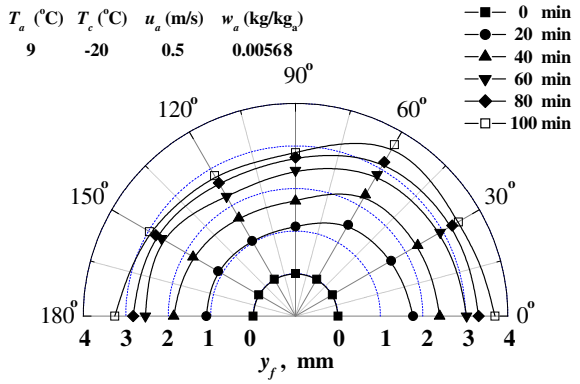

Fig. 3. Temporal variations in the frost thickness with angular position at a low air velocity.

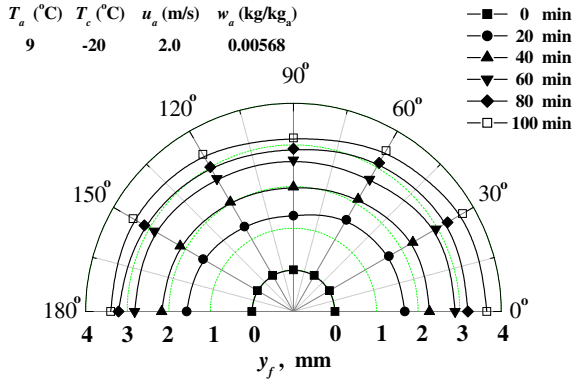

Fig. 4. Temporal variations in the frost thickness with angular position at a high air velocity.

Figs. 5 and 6 show the frost surface temperatures at each angular position under different air velocity conditions. The variations in the frost surface temperature with angular position were similar to those of the frost thickness. The frost surface temperature at the front of the cylinder was high due to the fast-growing frost layer and the collision of high-temperature air. However, the frost surface temperature at the rear of the cylinder for a low air velocity was

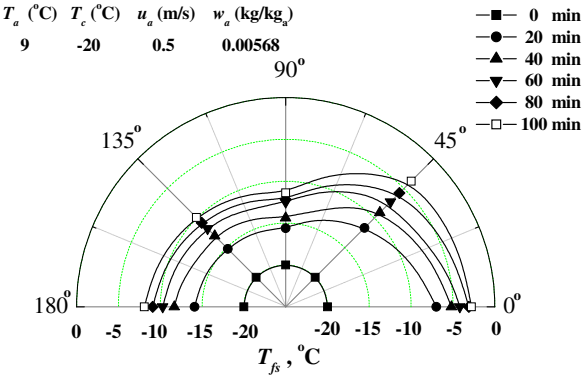

Fig. 5. Temporal variations in the frost surface temperature with angular position at a low air velocity.

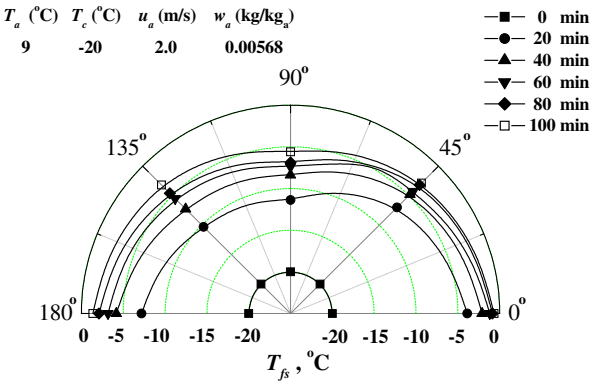

Fig. 6. Temporal variations in the frost surface temperature with angular position at a high air velocity.

low because of the slowly growing frost layer and lower surrounding air temperature.

The local frost densities for different air velocities are shown in Figs. 7 and 8. The frost layer at the front stagnation point was dense owing to the high frost surface temperature. However, the frost density at the rear stagnation point was much lower than that at the neighboring 90° intervals, despite the higher frost surface temperature at the rear stagnation point. Since the frost thickness increased with the generation and growth of the vortex flow despite the decreased mass transfer potential due to the low temperature and humidity of the air at the rear stagnation point, the frost density decreased in return.

3.2. Correlations

To analyze the effects of frost behavior on the frosting parameters, correlations were derived using the mean values of the local frost properties. The frost properties were expressed as functions of dimensionless frosting parameters using a dimensional analysis. The frosting parameters, measured frost properties, and selected parameters were included as variables in the dimensional analysis. The variables in the dimensional analysis were air temperature, air velocity, air humidity ratio, cold cylinder surface tempera-

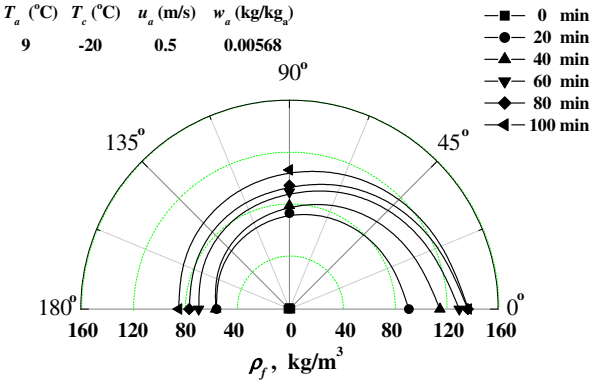

Fig. 7. Temporal variations in the frost density with angular position at a low air velocity.

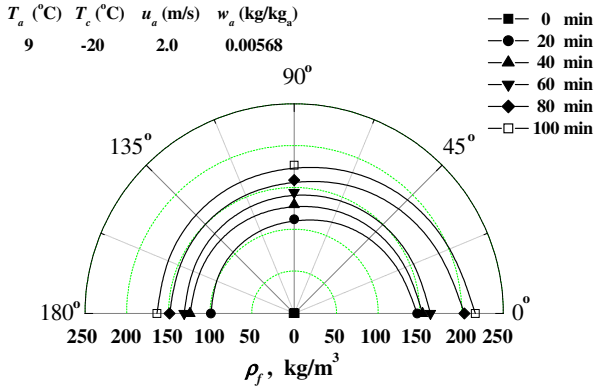

Fig. 8. Temporal variations in the frost density with angular position at a high air velocity.

ture, frosting time, frost thickness, frost density, frost surface temperature, heat transfer coefficient, diameter of the cylinder, density and thermal conductivity of the air, ice density, and triple point temperature of the water.

A general correlation for the frost properties was obtained from the dimensional analysis as follows:

$$f\left(y_{\mathrm{f}}^{*}, \rho_{\mathrm{f}}^{*}, T_{\mathrm{fs}}^{*}, Nu, Re_{\mathrm{d}}, Fo, w_{\mathrm{a}}, T_{\mathrm{a}}^{*}, T_{\mathrm{c}}^{*}\right) = 0 \tag{5}$$

where $y_{\mathrm{f}}^{*}, \rho_{\mathrm{f}}^{*}, T_{\mathrm{fs}}^{*}, T_{\mathrm{a}}^{*}$, and T_{c}^{*} represent, y_{f}/d, $\rho_{\mathrm{f}}/\rho_{\mathrm{ice}}$, $(T_{\mathrm{fs}} - T_{\mathrm{tp}})/(T_{\mathrm{a}} - T_{\mathrm{c}})$, $T_{\mathrm{a}}/T_{\mathrm{tp}}$, and $T_{\mathrm{c}}/T_{\mathrm{tp}}$, respectively.

The frost properties were expressed as functions of the Reynolds number, Fourier number, air humidity ratio, and dimensionless air and cold surface temperatures:

$$F = f\left(Re_{\mathrm{d}}, Fo, w_{\mathrm{a}}, T_{\mathrm{a}}^{*}, T_{\mathrm{c}}^{*}\right) \tag{6}$$

The empirical dimensionless correlations of the average frost properties on the cold cylinder surface were derived as follows:

$$y_{\mathrm{f}}^{*} = \frac{y_{\mathrm{f}}}{d} = 3.236(Re_{\mathrm{d}})^{4.447\times10^{-2}}(Fo)^{0.550}(w_{\mathrm{a}})^{1.267} \times (T_{\mathrm{a}}^{*})^{-14.884}(T_{\mathrm{c}}^{*})^{-8.400} \tag{7}$$

$$\rho_{\mathrm{f}}^{*} = \frac{\rho_{\mathrm{f}}}{\rho_{\mathrm{ice}}} = 4.264\times10^{-4}(Re_{\mathrm{d}})^{0.346}(Fo)^{0.208}(w_{\mathrm{a}})^{-0.398} \times (T_{\mathrm{a}}^{*})^{14.001}(T_{\mathrm{c}}^{*})^{4.678} \tag{8}$$

$$T_{\mathrm{fs}}^{*} = \frac{T_{\mathrm{fs}} - T_{\mathrm{tp}}}{T_{\mathrm{a}} - T_{\mathrm{p}}} = \frac{T_{\mathrm{p}} - T_{\mathrm{tp}}}{T_{\mathrm{a}} - T_{\mathrm{p}}} + 7.320(Re_{\mathrm{d}})^{0.312}(Fo)^{0.314} \times (w_{\mathrm{a}})^{1.337}(T_{\mathrm{a}}^{*})^{-12.980}(T_{\mathrm{c}}^{*})^{-8.021} \tag{9}$$

$$Nu_{\mathrm{ave}} = \frac{h_{\mathrm{h}}d}{k_{\mathrm{a}}} = 0.437(Re_{\mathrm{d}})^{0.431}(Fo)^{0.275}(w_{\mathrm{a}})^{-0.173} \times (T_{\mathrm{a}}^{*})^{-9.661}(T_{\mathrm{c}}^{*})^{7.221} \tag{10}$$

The applicable ranges of these correlations were $700 \leqslant Re_{\mathrm{d}} \leqslant 3000$ $(0.5 \leqslant u_{\mathrm{a}} \leqslant 2.0$ m/s), $56.8 \leqslant Fo \leqslant 295.7$ $(0 \leqslant t \leqslant 100$ min), $0.00280 \leqslant w_{\mathrm{a}} \leqslant 0.00568$ kg/kg$_{\mathrm{a}}$, $3 \leqslant T_{\mathrm{a}} \leqslant 9$ °C and $-32 \leqslant T_{\mathrm{c}} \leqslant -20$ °C.

Fig. 9 compares the measured and correlated data for the dimensionless frost properties, such as frost thickness, frost density, frost surface temperature, and Nusselt number. The proposed correlations agreed well with the experimental data, with a maximum error of 15%.

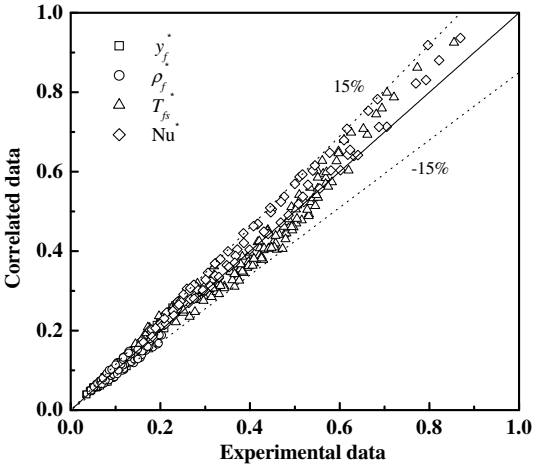

Fig. 9. Comparison of the measured and correlated data for the dimensionless frost properties.

Most research related to cylinders has predicted the thickness and density of the frost layer. Correlations for a cold cylinder are generally unavailable in the literature, and correlations that do exist do not apply to the same test conditions as the correlations proposed in this study. Thus, only the results of the thickness and density of the frost layer calculated from Eqs. (7) and (8) were compared with experimental data from previous studies [9,11,14] under similar ranges of test conditions, as shown in Figs. 10 and 11. The results from Lee and Ro [9] and Aoki et al. [11] are mean experimental values measured at different angular positions on the cylinder, and those of Schneider [14] are displayed as a function of time on a log–log plot. The proposed frost thickness correlations agreed with the experimental data from these previous studies, with a maximum error of 10%, and the proposed frost density correlation predicted the experimental data of Aoki et al. [11] well, with a maximum error of 15%.

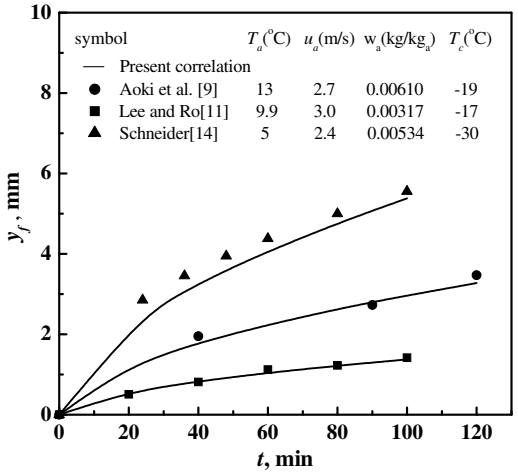

Fig. 10. Comparison of the proposed frost thickness correlation and experimental data from previous studies.

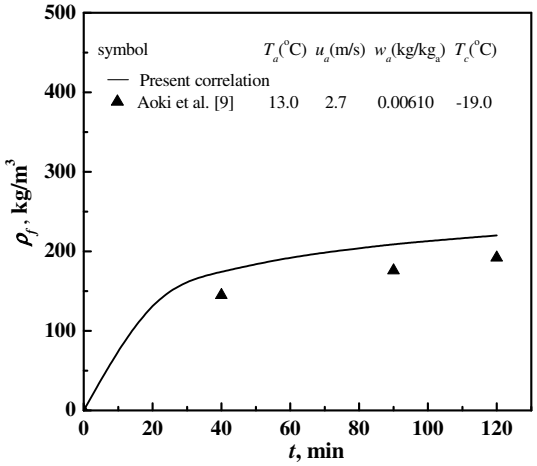

Fig. 11. Comparison of the proposed frost density correlation and experimental data from a previous study.

4. Conclusions

We investigated local frosting behavior on a horizontal cylinder surface through frosting experiments and proposed empirical dimensionless correlations of the frost properties. The experimental results showed that the local frost thickness at a high air velocity did not vary with angular position. The dimensionless correlations of the frost properties, such as the frost thickness, frost density, frost surface temperature, and heat transfer coefficient were derived as functions of the Reynolds number, Fourier number, absolute humidity, dimensionless air temperature, and dimensionless cold surface temperature. The proposed correlations are applicable for Reynolds number of 700–3000 (air velocities of 0.5–2.0 m/s), Fourier number of 56.8–295.7 (operating time of 0–100 min), absolute humidity of 0.00280–0.00568 kg/kg$_a$, air temperatures of 3–9 °C, and cold cylinder surface temperatures of −32 to −20 °C. The proposed correlations agreed well with the experimental data, with a maximum error of 15%.

Acknowledgement

This research was supported by The Center of Innovative Design Optimization Technology (iDOT), Korea Science and Engineering Foundation.

References

[1] R. Östin, S. Anderson, Frost growth parameters in a forced air stream, Int. J. Heat Mass Transfer 14 (4/5) (1991) 1009–1017.
[2] J.D. Yonko, C.F. Sepsy, An investigation of the thermal conductivity of frost while forming on a flat horizontal plate, ASHRAE Trans. 73 (2) (1967) 1.1–1.11.
[3] I. Tokura, H. Saito, K. Kishinami, Study on properties and growth rate of frost layers on cold surfaces, J. Heat Transfer 105 (1983) 895–901.
[4] G. Biguria, L.A. Wenzel, Measurement and correlation of water frost thermal conductivity and density, I&EC Fund. 9 (1) (1970) 129–138.
[5] T. Hosoda, H. Uzuhashi, Effects of frost on the heat transfer coefficient, Hitachi Rev. 16 (6) (1967) 254–259.
[6] Y. Mao, R.W. Besant, K.S. Rezkallah, Measurement and correlations of frost properties with airflow over a flat plate, ASHRAE Trans. Res. 91 (1992) 267–281.
[7] Y. Mao, R.W. Besant, H. Chen, Frost characteristics and heat transfer on a flat plate under freezer operating conditions: Part 1, Experimentation and correlations, ASHRAE Trans. Res. 105 (2) (1999) 231–251.
[8] D.K. Yang, K.S. Lee, Dimensionless correlations of frost properties on a cold plate, Int. J. Refrig. 27 (1) (2004) 89–96.
[9] H. Aoki, N. Yamakawa, S. Ohtani, Forced convective heat transfer around a vertical cylinder under frosting conditions, Heat Transfer-Jpn. Res. 1 (1981) 53–63.
[10] P.M. Chung, A.B. Algren, M. Minneapolis, Frost formation and heat transfer on a cylinder surface in humid air cross flow, Heat., Piping, Air Cond. 30 (9) (1958) 171–178.
[11] Y.B. Lee, S.T. Ro, An experimental study of frost formation on a horizontal cylinder under cross flow, Int. J. Refrig. 24 (2001) 468–474.
[12] M.M. Padki, S.A. Sherif, R.M. Nelson, A simple method for modeling the frost formation phenomenon in different geometries, ASHRAE Trans. 95 (2) (1989) 1127–1137.
[13] C.J. Cremers, V.K. Mehra, Frost formation on vertical cylinders in free convection, ASME J. Heat Transfer 104 (1) (1982) 3–7.
[14] H.W. Schneider, Equation of the growth rate of frost forming on cooled surfaces, Int. J. Heat Mass Transfer 21 (1978) 1019–1024.
[15] S. Sengupta, S.A. Sherif, K.V. Wong, Empirical heat transfer and frost thickness correlations during frost deposition on a cylinder in cross-flow in the transient regime, Int. J. Energ. Res. 22 (1998) 615–624.
[16] S.J. Kline, F.A. McClintock, Describing uncertainties in single-sample experiments, Mech. Eng. 75 (1953) 3–8.
[17] F.P. Incropera, D.P. DeWitt, Fundamental of Heat and Mass Transfer, John Wiley and Sons Inc., 2002, pp. 407–413.